Nanoscale

Volume 1 | Number 1 | Jan 2013 | Pages 1–100

Nanoscale

www.rsc.org/nanoscale

ROYAL SOCIETY OF CHEMISTRY

This is an *Accepted Manuscript*, which has been through the Royal Society of Chemistry peer review process and has been accepted for publication.

Accepted Manuscripts are published online shortly after acceptance, before technical editing, formatting and proof reading. Using this free service, authors can make their results available to the community, in citable form, before we publish the edited article. We will replace this *Accepted Manuscript* with the edited and formatted *Advance Article* as soon as it is available.

You can find more information about *Accepted Manuscripts* in the **Information for Authors**.

Please note that technical editing may introduce minor changes to the text and/or graphics, which may alter content. The journal's standard **Terms & Conditions** and the **Ethical guidelines** still apply. In no event shall the Royal Society of Chemistry be held responsible for any errors or omissions in this *Accepted Manuscript* or any consequences arising from the use of any information it contains.

ROYAL SOCIETY OF CHEMISTRY

www.rsc.org/nanoscale

Journal Name

ARTICLE

The Effect of Surface Passivation on the Structure of Sulphur-Rich PbS Colloidal Quantum Dots for Photovoltaic Application

Victor Malgras,[a] Andrew Nattestad,[b,*] Yusuke Yamauchi,[c] Shi Xue Dou[a] and Jung Ho Kim[a,*]

The use of PbS colloidal quantum dots in photovoltaic devices is very promising because of their simple and low cost production processes and their unique properties such as bandgap tunability and potential multiple exciton generation. Here we report the synthesis of PbS nanocrystals used for application in solar cells. The sulphur-rich nature of their surface appears to be caused by the exposure to ambient conditions. The use of methanol as medium during the ligand exchange process has a crucial role in the removal of native oleate ligands. Without proper ligand exchange, the unpassivated surface is subject to ambient hydroxylation leading to the depletion of Pb atoms and the formation of a polysulfide phase. Devices assembled with this material showed good performance with an efficiency of 3.2%.

Introduction

Colloidal nanocrystals of semiconducting materials with a size smaller than the Bohr radius of their exciton, also known as "quantum dots (QDs)", are well known for their unique electronic and optical properties, differing from their bulk counterparts due to their small size. These nano-structures have attracted considerable attention due to their size-dependent optical band-gap[1, 2] and their ability to generate multiple excitons from a single photon.[3] These properties have provided motivation for their application in a wide range of optoelectronic devices. Recently, solar cells based on the *p-n* junction between a wide band-gap *n*-type semiconductor (*eg.* TiO$_2$, ZnO) and a *p*-type lead-rich PbS colloidal quantum dot (CQD) film have been reported with solar-to-electric conversion efficiencies reaching 7%.[4, 5] Prior to device assembly, the nanocrystals are embedded in long-chain, coordinating, ligands (i.e., oleates) for three main reasons: it provides stable suspension in non-polar solvent, prevents aggregation and protect the surface from adventitious atmospheric contamination (i.e., oxygen and moisture). In order to improve electron transfer through the quantum dot film, however, these bulky molecules have to be replaced by shorter ligands to reduce the inter-particle distance while maintaining a certain degree of protection. So far, this has been achieved by treating the cast CQD film with small carboxylic acid containing molecules dissolved in methanol. This ligand exchange is a critical step in the device assembly as it ensures charge transport can occur while maintaining the quantum-confinement-dependent-properties. The mechanisms of this ligand removal process are not well understood, however. In this work, we provide a thorough structural study of the surface of sulphur-rich PbS CQDs passivated with oleic acid, before and after treatment with methanol. This study employs transmission electron microscopy (TEM) in conjunction with X-ray photoelectron spectroscopy (XPS) analysis in order to develop a better understanding of the processes involved in ligand exchange.

Experimental method

Synthesis of PbS CQDs. All the chemicals were obtained from Sigma-Aldrich (with the exception of oleic acid from Alfa Aesar) and were used without further purification. The synthesis was adapted from previously reported procedures.[6, 7] 2 mmol PbO (99.9%) was dissolved in a solution of 1.5 mL oleic acid (90%) and 10 mL 1-octadecene (90%) under vacuum and with vigorous stirring at 90 °C using an oil bath. The precursor turned clear after 4 hours and the temperature was set at 118 °C. A solution of 1 mmol bis(trimethylsilyl)sulphide diluted in 5 mL 1-octadecene was rapidly injected and the hotplate was turned off to let the flask cool down naturally to room temperature. The product was precipitated with acetone (anhydrous), centrifuged, dispersed in toluene (anhydrous) and reprecipitated three times. It was finally dispersed in n-octane at 45 mg/mL concentration for further use. The whole process was carried under ambient conditions.

Material characterization. A carbon coated copper TEM grid was dipped in a diluted (0.2 mg/mL) PbS CQDs solution in n-octane and was analysed using a double aberration-corrected JEOL JEM-ARM 200F TEM equipped with both probe and image correctors. The methanol treatment consisted of dropping 50 µL of methanol (anhydrous) on the PbS CQDs coated TEM grid. Excess solvent was removed using absorbing paper. X-ray diffraction (XRD) was carried out with a GBC-MMA diffractometer at a rate of 0.05°/s. Energy dispersive spectroscopy (EDS) was conducted by using a JEOL JED-2300 30 mm^2, 144 eV Mini-Cup SiLi detector on a JEOL JSM-6490LA scanning electron microscope. For XPS analysis, the single layer of PbS CQDs was spincast on a 10 mm × 10 mm (100)-Si wafer at 2500 rpm for 10 s. The methanol treatment consisted in a subsequent spinpcast of 0.5 mL of methanol at 2500 rpm for 10 s. The XPS measurement was conducted using a SPECS PHOIBOS 100 Analyser installed in a high-vacuum chamber with base pressure below 10^{-8} mbar. X-ray excitation through Al Kα radiation (hv = 1486.61 eV) was operated at 12 kV (120 W). The XPS binding energy high resolution spectra were collected with a 20 eV pass energy in the fixed analyser transmission mode. The calibration was performed by fitting the C 1s and Cu 2p peaks from a pure copper sample. Analysis of the XPS data was carried out using the commercial CasaXPS2.3.15 software package. The signal was fitted using a Voigt Gauss-Lorentz (GL) line shape, GL(30), and the background type was set to "Shirley". The Pb $4f_{7/2}$/Pb $4f_{5/2}$ and S $2p_{3/2}$/S $2p_{1/2}$ doublet fittings were forced with an energy difference of 4.86 eV and 1.18 eV and an area ratio of 4:3 and 2:1, respectively.[8] The number of peaks added in the convolution was kept to the minimum which could bring a satisfactory residual fitting. For the sake of clarity, only the main component of each doublet is identified on the graph. A general survey scan was always performed in order to confirm that no silicon peak from the substrate appears, ensuring that the emitted photoelectrons are only coming from the CQD film.

Device fabrication and characterization. 100 nm of a TiO$_2$ dense layer was deposited on fluorine doped tin oxide (FTO) glass through spray pyrolysis of titanium diisopropoxide bis(acetylacetonate) (75% in isopropanol).[9] PbS CQDs were deposited in a layer-by-layer manner, with 100 µL of CQD suspension applied at 2500 rpm for 10 seconds, followed by spincasting of a methanolic solution of 3-mercaptopropionic acid (2% v/v) and rinsed abundantly with methanol and then heptane. The sample was placed in a vacuum chamber (10^{-7} mbar) where 10 nm molybdenum oxide (MoO$_x$) film followed by 70 nm gold film were deposited through thermal evaporation. The devices were then brought into an argon-filled glove box, where they were sealed with a poly(methyl methacrylate) cavity and reactive epoxy (retaining an argon pocket). The incident photon-to-charge carrier efficiency (IPCE) was measured using Oriel® Newport Instrument monochromators and a Keithley 2400 connected to a computer running a modified LabVIEW® software. The current density-voltage (*J-V*) curves were obtained under illumination from a class AAA Peccell Xenon lamp solar simulator (PEC-L12).

Results and Discussion

Fig. 1 shows high resolution TEM (HRTEM) images of highly crystalline PbS CQDs with and without methanol treatment. In Fig. 1a, the lattice fringes of randomly oriented crystals can be seen, allowing one to measure particle sizes. Although, due to agglomeration in sample preparation, exact interparticle spacing was
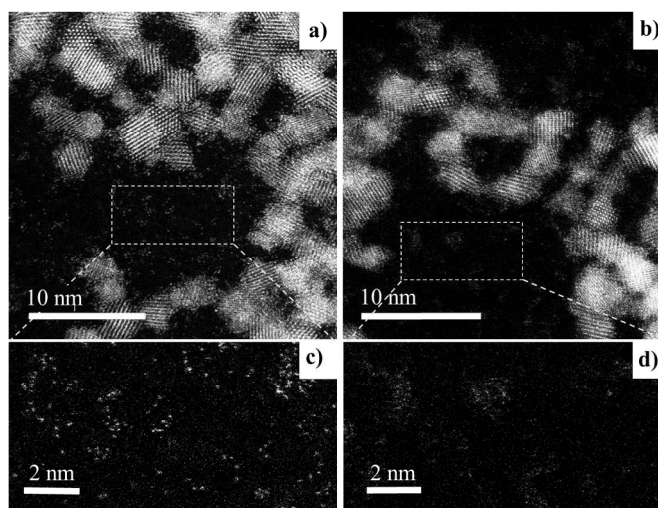

Fig. 1 HRTEM images of highly crystalline PbS CQDs without treatment (a) and treated with methanol (b). c) and d) are enlargements of the dark area without nanocrystals from (a) and (b), respectively.

not able to be observed. The methanol treatment did not appear to alter the shape or size of the CQDs. It can, however, be observed that the methanol treated sample (see Fig. 1b) has significantly more amorphous material. The untreated sample also contains numerous impurities, as can be observed in Fig. 1c. The brightness of these particles is most likely due to heavy atoms such as Pb which may be present in the form of residual lead oleate (Pb-OL$_2$), from the particle synthesis, despite the washing steps that were performed. Due to the precursor and the CQDs having similar solubilities, they are difficult to separate from one another. After methanol treatment (Fig. 1d), the dark regions only display pale shades, which could be assigned to organic materials (e.g. oleic acid), but no presence of lead was observed. This supports the observation of Cass et al. who previously reported that acetone wash, unlike methanol, could not remove all the oleate clusters.[10]

The histogram in Fig. 2a confirms the narrow size distribution of the particles as observed in Fig. 1a, with a mean diameter of 3.2 nm and a relative standard deviation of 7.2%. This is also reflected in the sharp absorption peak at 937 nm (1.32 eV) due to the first exciton transition energy (see Fig. 2a inset), in accordance with the quantum confinement model of Kang et al.[11] The CQDs appear to be mostly
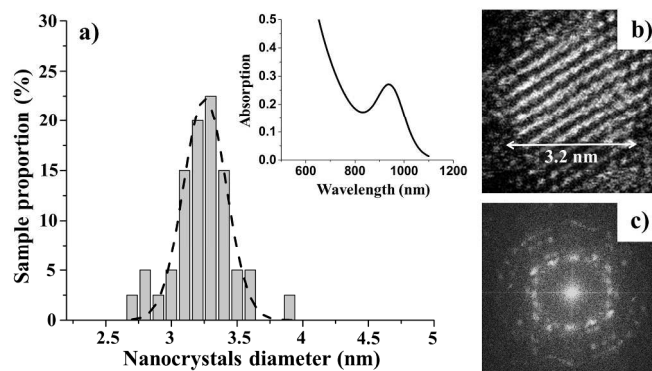

Fig. 2 a) Size distribution of nanocrystals measured from Fig. 1 (a). The inset is the typical optical absorption spectrum. b) Enlargement of a single nanocrystal. The inset is the typical absorption spectrum. c) Fourier transform of Fig. 1 (a).
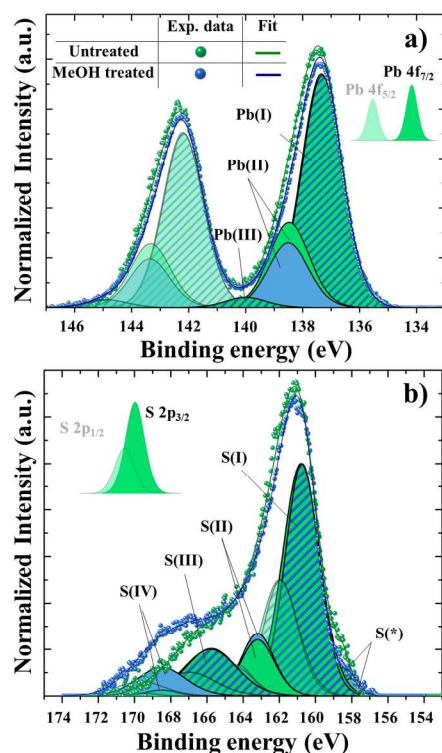
Table 1 Attribution of the features from the Pb $4f_{7/2}$ spectrum

Feature label	Binding energy (eV)	Attribution
Pb(I)	137.3	Pb-S
Pb(II)	138.5	Pb-OL$_2$, S-Pb-OL, PbSO$_3$, Pb(OH)$_2$
Pb(III)	140.0	PbSO$_4$

contributions (see Table 1). The methanol treatment appears to have a negligible effect except for a small reduction of the Pb(II) contribution at 138.5 eV. This correlates with the assumption that some unreacted Pb-OL$_2$, present initially, will be washed away during the treatment, as can be inferred from Fig. 1c and Fig. 1d. It is suspected, however, that oxidized or hydroxylated species such as PbSO$_3$ and Pb(OH)$_2$ could also be present and have their contribution within the window of 138.5 ± 0.5 eV.

The S 2p fitting is more complex due to the sulphur rich character of the surface of the nanocrystals and could not be properly fitted using less than five species (Table 2). In Fig. 3b, the most prominent feature, S(I) at 160.7 eV, is attributed to S bound to Pb (in a rock-salt type formation). It overlaps, however, with a smaller peak S(*) at 158.2 eV which is related to energy loss from Pb 4f and therefore, is excluded from the quantitative analysis of sulphur species content.[15] S(II) at 163.2 eV is assigned to sulphur involved in S-S bonds while S(III) and S(IV) located at 168.1 eV and 170.5 eV are assigned to oxidized species such as SO$_3$ and SO$_4$, respectively. The latter two are broader due to different phonon relaxation mechanisms taking place at the surface, as previously reported.[16-18] Both samples reveal similar features, except for a significant increase of the S(IV) content in the treated sample, confirming the importance of the oleate
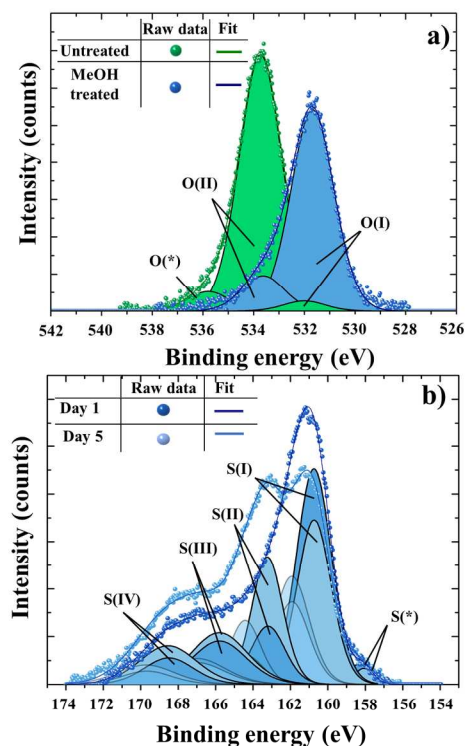
Fig. 3 High resolution XPS spectra centred on Pb 4f (a) and S 2p (b) doublets. The green and blue filled peaks are the deconvoluted species from the fits for the untreated and methanol treated samples, respectively. The striped peaks indicates a complete overlap between the two samples. The insets are a visual help to dissociate each component of the doublets. The semi-transparent peaks are attributed to the minor component of the doublet used for the fitting and should be disregarded for the analysis.

spherical (Fig. 2b) with negligible lattice distortion. Four characteristic interplanar spacings were identified through the electron diffraction pattern corresponding to the 111, 002, 220 and 311 planes (Fig. 2c). The *d*-spacing for each of these planes is within 5% variation of that predicted by XRD (see Fig. S1 in the Supporting Information).

XPS analysis was carried out in order to ascertain the overall stoichiometry of the system. It was found that the nanocrystal films were sulphur rich with a S:Pb ratio close to 2:1. This was also confirmed by EDS measurements both before (65.8 at.% S) and after treatment (67.7 at.% S). This composition is rather different than what other authors reported for similar materials[4, 12-14] and can arise from alterations of the synthesis process or from post-synthetic exposure to atmospheric conditions. The excess sulphur content, however, does not affect the PbS rock salt crystallinity of the quantum dots, as confirmed in Fig. 1 and Fig. 2. For this reason, it is assumed that this composition mostly reflects a surface rich in sulphur, while the core retains a bulk-like S:Pb ratio of 1:1.

The signal intensities for both Pb and S are significantly reduced by the presence of abundant oleate ligands in the untreated sample. In order to observe the impact of the methanol treatment on the presence of these elements, the high-resolution XPS spectra were normalized using the "core" Pb-S bond peaks as reference (Pb(I) and S(I) for Pb 4f and S 2p, respectively), since the "core" features are the least likely to be altered by the treatment. In general, the significant line broadening is due to instrumental limitations. In Fig. 3a, the fitting of Pb $4f_{7/2}$ is deconvoluted into three major

Fig. 4 (a) High resolution XPS spectra centred on O 1s (a) for both the treated and untreated samples. (b) S 2p of the treated sample before and after exposure to atmospheric conditions for 5 days.

Table 2 Attribution of the features from the S 2p$_{3/2}$ spectrum

Feature label	Binding energy (eV)	Attribution
S(I)	160.7	S-Pb
S(II)	163.2	S_n^{2-} (polysufide)
S(III)	165.8	SO_3-Pb
S(IV)	168.5	SO_4-Pb
S(*)	*158.2*	*Pb 4f energy loss feature*

molecules as a capping agent protecting the surface from adventitious oxidation mechanisms.

The O 1s peak in Fig. 4a is divided into three contributions (see Table 3). O(I) at 531.8 eV is assigned to –OH groups,[19, 20] which would most likely be found in the form of $Pb(OH)_2$. O(II), at 533.6 eV, is assigned to carboxylate groups, attributed to oleate molecules surrounding the nanocrystals, while O(*) is a weak satellite assigned to excitations related to carboxylate groups.[21] This is confirmed by the presence of a similar peak (with ~ 2.1 eV energy separation from the carboxylate contribution) on the C 1s spectrum (see Fig. S2 in the Supporting Information).

After the films were aged in unprotected atmospheric conditions (with an ambient relative humidity of 50-60%), the untreated sample shows relatively little change in the S 2p contributions (see Fig. S3 in the Supporting Information) compared with the treated one (Fig. 4) where a significant trade-off can be observed between S(I), with the concentration dropping from 57% to 38%, and S(II) increasing from 15% to 27%. This suggests that a significant proportion of the sulphur, contained under the surface as PbS, has a different electronic configuration after atmospheric exposure. This can be explained in terms of exposure to both water (atmospheric humidity) and oxygen: [22, 23]

$$PbS + 1/2\,x O_2 + x H_2O \rightarrow Pb_{1-x}S + x Pb(OH)_2$$
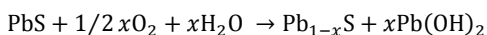
The presence of $Pb(OH)_2$ is confirmed by the O(I) peak, but the resolution of the instrument could not deconvolve the Pb-OH contribution from Pb-OL_2 or $PbSO_3$.

The remaining phase at the surface of the nanocrystal, $Pb_{1-x}S$, is lead-deficient, as was confirmed by the high S:Pb atomic ratio obtained through XPS and EDS. Such vacancies induce the sulphur to rebuild as polysulphide (S_n^{2-}) groups,[24, 25] which explains why the S-S bond contribution is about 0.7 eV lower than what could be expected for elemental sulphur (S_0).[8] The relatively small change in the polysulphide contribution of the methanol-treated sample before exposure to ambient conditions indicates that the lead atoms have not been displaced, and thus, the treatment is successful in the removal of the oleate tails which are passivating/protecting these sites from hydroxylation.

Devices assembled with sulphur-rich PbS CQD films display relatively high external quantum efficiencies (~ 65% at 420 nm) and reflect the PbS absorption profile (see Fig. 5a), including the

Table 3 Attribution of the features from the O 1s spectrum

Feature label	Binding energy (eV)	Attribution
O(I)	531.8	Pb-O-H
O(II)	533.6	COO^-
O(*)	535.7	Satellite

aforementioned excitonic peak (redshifted to around 1000 nm in the film). Initially, the device showed high short-circuit current density J_{SC} (above 20 mA/cm^2) with an open-circuit voltage, V_{OC}, of 0.41 V, a fill factor of 0.40 and an overall power efficiency of 3.2%. Despite the encapsulation, repeated measurements revealed stability issues. Testing revealed both reversible and irreversible degradation processes. Interestingly, different parameters were altered differently during the tests; in particular V_{OC} was the most affected with a decrease of approximately 40 mV/sweep under illumination. When the device was kept in the dark for two hours, V_{OC} remained unchanged, unlike J_{SC} which continued decreasing (albeit at a slower rate). After one day, in the dark and under open circuit conditions the device showed a full recovery and maintained its maximum power efficiency for a further week before undergoing irreversible degradation. After 1 month, a drop of 77% in J_{SC} and 60% in V_{OC} could be observed (see Fig. S4 in the Supporting Information).

The performance of these devices is comparable to what was reported over the last 3 years.[4, 26-29] Such stability matters, however, have received very little, if any, attention in these publications. It is believed that they could be related to the different surface stoichiometry of the material used in the present work. Indeed, it was reported that 3-mercaptopropionic acid coordinates to the nanocrystals through both groups: thiol and carboxylate.[30] These groups can only form ionic bonding with the positive lead ions. The sulphur-rich character of the present films is expected to have considerable impact on the effective ligand coverage and thus, the performance and stability of the device. Improved stability could be achieved by maintaining the whole assembly process in a controlled dry atmosphere, as well as by developing passivation methods that would be suitable to protect sulphur-rich surfaces from degradation. Also, further experiments are planed aiming to understand the role of
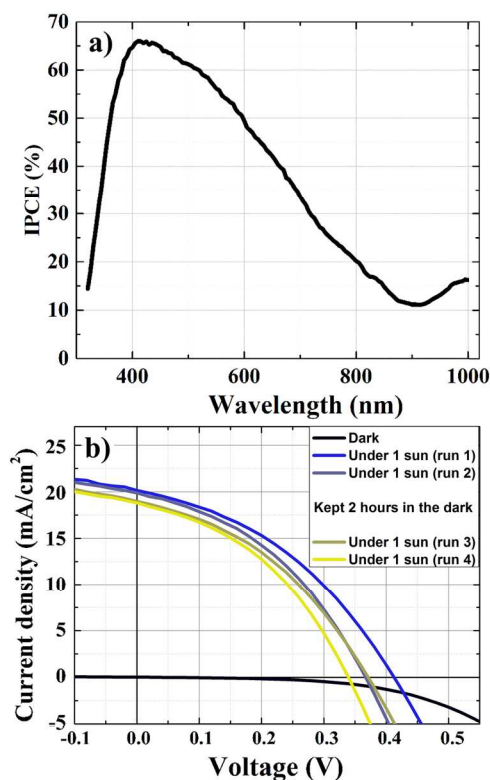
Fig. 5 IPCE spectrum (a) and J-V curve under both dark and light conditions (b) of a sulphur-rich PbS CQD solar cell.

illumination, bias and time on the impact on the overall performance of the cell.

Conclusions

Lead sulphide (PbS) nanocrystals were synthesized with a mean size of 3.2 nm. TEM and XRD reveals that the bulk PbS has a rock-salt symmetry, while XPS indicates that they are sulphur-rich at the surface, which is assumed to be due to surface depletion of Pb-following a hydroxylation process (resulting from exposure to atmospheric conditions). Methanol treatment appears to have a decisive role in the removal of oleate tails, thus facilitating the exchange with shorter ligand molecules. In the absence of a new capping agent, the surface is left mostly unpassivated and lead atoms from the PbS lattice are slowly removed to leave a Pb-deficient polysulphide phase. Devices made from this material show good photovoltaic performances initially with photocurrents up to 20.1 mA/cm^2 and an efficiency of 3.2%. They display short-term stability issues, however, as both the current and the voltage slowly decrease during measurements under light exposure. Although their performance could be fully recovered after being kept in the dark for a day, the device shows sign of irreversible degradation after a week.

Acknowledgements

Notes and references

^{a} Institute for Superconducting and Electronic Materials (ISEM), University of Wollongong, North Wollongong, NSW 2500, Australia
Email: jhk@uow.edu.au
^{b} ARC Centre of Excellence for Electromaterials Science, Intelligent Polymer Research Institute (IPRI), University of Wollongong, North Wollongong, NSW 2500, Australia
Email: Anattest@uow.edu.au
^{c} National Institute for Materials Science (NIMS), 1-1 Namiki, Tsukuba, Ibaraki 305-0044, Japan

1. A. P. Alivisatos, *Science*, 1996, **271**, 933-937.
2. X. Wang, J. Zhuang, Q. Peng and Y. Li, *Nature*, 2005, **437**, 121-124.
3. R. J. Ellingson, M. C. Beard, J. C. Johnson, P. R. Yu, O. I. Micic, A. J. Nozik, A. Shabaev and A. L. Efros, *Nano Lett.*, 2005, **5**, 865-871.
4. J. Tang, L. Brzozowski, D. A. R. Barkhouse, X. Wang, R. Debnath, R. Wolowiec, E. Palmiano, L. Levina, A. G. Pattantyus-Abraham, D. Jamakosmanovic and E. H. Sargent, *ACS Nano*, 2010, **4**, 869-878.
5. A. H. Ip, S. M. Thon, S. Hoogland, O. Voznyy, D. Zhitomirsky, R. Debnath, L. Levina, L. R. Rollny, G. H. Carey, A. Fischer, K. W. Kemp, I. J. Kramer, Z. Ning, A. J. Labelle, K. W. Chou, A. Amassian and E. H. Sargent, *Nat. Nanotechnol.*, 2012, **7**, 577-582.
6. C. B. Murray, S. H. Sun, W. Gaschler, H. Doyle, T. A. Betley and C. R. Kagan, *IBM J. Res. Dev.*, 2001, **45**, 47-56.
7. M. A. Hines and G. D. Scholes, *Adv. Mater.*, 2003, **15**, 1844-1849.
8. J. F. Moulder, W. F. Stickle, P. E. Sobol and K. D. Bomben, *Handbook of X-ray Photoelectron Spectroscopy*, Perkin-Elmer Corp., Eden Prairie, MN, 1992.
9. L. Kavan and M. Grätzel, *Electrochim. Acta*, 1995, **40**, 643-652.
10. L. C. Cass, M. Malicki and E. A. Weiss, *Anal. Chem.*, 2013, **85**, 6974-6979.
11. I. Kang and F. W. Wise, *J. Opt. Soc. Am. B: Opt. Phys.*, 1997, **14**, 1632-1646.
12. H. Choi, J.-H. Ko, Y.-H. Kim and S. Jeong, *J. Am. Chem. Soc.*, 2013, **135**, 5278-5281.
13. I. Moreels, K. Lambert, D. Smeets, D. De Muynck, T. Nollet, J. C. Martins, F. Vanhaecke, A. Vantomme, C. Delerue, G. Allan and Z. Hens, *ACS Nano*, 2009, **3**, 3023-3030.
14. C. Giansante, L. Carbone, C. Giannini, D. Altamura, Z. Ameer, G. Maruccio, A. Loiudice, M. R. Belviso, P. D. Cozzoli, A. Rizzo and G. Gigli, *J. Phys. Chem. C*, 2013, **117**, 13305-13317.
15. D. S. Zingg and D. M. Hercules, *J. Phys. Chem.*, 1978, **82**, 1992-1995.
16. J. Leiro, K. Laajalehto, I. Kartio and M. Heinonen, *Surf. Sci.*, 1998, **412**, L918-L923.
17. A. Lobo, T. Möller, M. Nagel, H. Borchert, S. G. Hickey and H. Weller, *J. Phys. Chem. B*, 2005, **109**, 17422-17428.
18. J. Akhtar, M. A. Malik, P. O'Brien, K. Wijayantha, R. Dharmadasa, S. J. Hardman, D. M. Graham, B. F. Spencer, S. K. Stubbs and W. R. Flavell, *J. Mater. Chem.*, 2010, **20**, 2336-2344.
19. D. T. Clark, B. J. Cromarty and A. Dilks, *J. Polym. Sci., Part A: Polym. Chem.*, 1978, **16**, 3173-3184.
20. Z. W. Li and Y. F. Zhu, *Appl. Surf. Sci.*, 2003, **211**, 315-320.
21. G. Jones, L. Jones, F. Thibault-Starzyk, E. Seddon, R. Raval, S. Jenkins and G. Held, *Surf. Sci.*, 2006, **600**, 1924-1935.
22. A. Buckley and R. Woods, *J. Appl. Electrochem.*, 1996, **26**, 899-907.
23. A. N. Buckley and R. Woods, *Appl. Surf. Sci.*, 1984, **17**, 401-414.
24. C. A. Prestidge and J. Ralston, *J. Colloid Interface Sci.*, 1995, **172**, 302-310.
25. R. S. C. Smart, W. M. Skinner and A. R. Gerson, *Surf. Interface Anal.*, 1999, **28**, 101-105.
26. J. B. Gao, J. M. Luther, O. E. Semonin, R. J. Ellingson, A. J. Nozik and M. C. Beard, *Nano Lett.*, 2011, **11**, 1002-1008.
27. A. G. Pattantyus-Abraham, I. J. Kramer, A. R. Barkhouse, X. Wang, G. Konstantatos, R. Debnath, L. Levina, I. Raabe, M. K. Nazeeruddin and M. Gratzel, *ACS Nano*, 2010, **4**, 3374-3380.
28. X. Wang, G. I. Koleilat, J. Tang, H. Liu, I. J. Kramer, R. Debnath, L. Brzozowski, D. A. R. Barkhouse, L. Levina and S. Hoogland, *Nat. Photonics*, 2011, **5**, 480-484.
29. R. Debnath, J. Tang, D. A. Barkhouse, X. Wang, A. G. Pattantyus-Abraham, L. Brzozowski, L. Levina and E. H. Sargent, *J. Am. Chem. Soc.*, 2010, **132**, 5952-5953.
30. K. S. Jeong, J. Tang, H. Liu, J. Kim, A. W. Schaefer, K. Kemp, L. Levina, X. Wang, S. Hoogland, R. Debnath, L. Brzozowski, E. H. Sargent and J. B. Asbury, *ACS Nano*, 2012, **6**, 89-99.